

Crystal Structure and Experimental and Theoretical Studies of the Second-Order Nonlinear Optical Properties of Salts of Triphenylguanidine with Carboxylic Acids

Pedro S. Pereira Silva,^{*,†} Cláudia Cardoso,[‡] Manuela Ramos Silva,[†] José A. Paixão,[†]
Ana Matos Beja,[†] Maria Helena Garcia,[¶] and Nelson Lopes[§]

CEMDRX, Physics Department, University of Coimbra, P-3004-516 Coimbra, Portugal, CFC, Physics Department, University of Coimbra, P-3004-516 Coimbra, Portugal, Faculdade de Ciências da Universidade de Lisboa, Ed. C8 Campo Grande, P-1749-016 Lisbon, Portugal, and GoLP/Centro de Física de Plasmas, Instituto Superior Técnico, P-1049-001 Lisbon, Portugal

Received: September 17, 2009; Revised Manuscript Received: December 23, 2009

N,N',N''-triphenylguanidinium carboxylate salts have been prepared by acid–base reactions of triphenylguanidine with formic, benzoic, and *m*-methoxybenzoic acids, and their single-crystal X-ray structure analysis has been performed. The salts were found to crystallize into noncentrosymmetric structures with an orthorhombic space group $P2_12_12_1$ for the formate and *m*-methoxybenzoate salts and a monoclinic space group Cc for the benzoate salt. The anions and cations are linked by intermolecular hydrogen bonds with the same motifs in the three salts. By using the molecular structures, the molecular first hyperpolarizabilities of several clusters were determined by semiempirical methods, and the components of the second-order susceptibility tensor, d , of triphenylguanidine and those of the reported crystals were evaluated using the oriented gas model with two different local-field corrections. The efficiency of the second-harmonic generation of triphenylguanidine and that of the reported triphenylguanidinium salts were measured using the Kurtz and Perry powder method.

1. Introduction

For the past three decades, organic materials that show quadratic nonlinear optical (NLO) properties have received considerable attention due to their promising potential applications in optical signal processing.^{1,2} In particular, measurements of the second-order NLO effect, second-harmonic generation (SHG), on certain organic NLO compounds have produced results that by far exceed those obtained from inorganic NLO alternatives such as lithium niobate (LiNbO_3) or potassium dihydrogen phosphate (KDP).^{3,4} Organic materials offer other advantages over conventional inorganic NLO materials, including fast response times, high optical damage thresholds, and much greater versatility in molecular design compared with their inorganic counterparts, thereby providing many more opportunities for improving the SHG response.

However, purely organic compounds in which van der Waals interactions dominate lack sufficient mechanical strength and thermal stability for practical uses. That is why we have used recently a crystal engineering strategy based essentially on the crystallization of ionic salts to get more cohesive crystalline structures. One aspect of particular interest with organic salts is the use of counterion variations to tailor crystal packing, potentially producing noncentrosymmetric bulk structures which are essential for quadratic NLO effects. Furthermore, crystalline salts possess inherently greater stabilities and higher chromophore number densities than potential alternatives for NLO device applications such as poled polymer materials. Within this crystal engineering strategy, several success cases have been reported, for instance, the DAST (4-*N,N*-dimethylamino-4'-*N'*-

methyl-stilbazolium tosylate) crystal^{3,5} and the NPP (*N*-(4-nitrophenyl)-(L)-prolinol) crystal,⁶ which led to the first demonstration of a near-IR optical parametric oscillation in an organic crystal.⁷ One should also cite the role of chirality (the use of natural amino acid derivatives) to prevent centrosymmetry with certainty; see, for example, the case of MAP (methyl-(2,4-dinitrophenyl)aminopropanoate) crystal.⁸

A second-order NLO chromophore typically contains a conjugated π -electron system, asymmetrically substituted by electron donor and acceptor groups, through which a charge transfer occurs. In such systems, the dominant first hyperpolarizability component is along the direction of charge transfer. The antiparallel alignment of the dipole moments of one-dimensional chromophores leads the majority of π -conjugated organic molecules to crystallize in centrosymmetric space groups, having therefore null second-order bulk susceptibility. One of the solutions to achieve dipole minimization without losing the molecular hyperpolarizability is the use of octupolar systems since their symmetry ensures cancellation of the molecular dipole moment.^{9,10} Furthermore, a noncentrosymmetric octupolar structure facilitates an optimal transfer of the molecular hyperpolarizability components to the macroscopic level,^{11,12} as exemplified in the TTB (1,3,5-tricyano-2,4,6-tris(*p*-diethylaminostyryl)benzene) crystal.¹³

Guanidine derivatives can be regarded as potentially interesting for quadratic NLO applications, as was demonstrated in 1993 by Zyss et al. with the encapsulation of guanidinium cations between hydrogen L-tartrate anions.¹⁴

Triphenylguanidine (TPG) is easily protonated, and its cationic form is capable of forming ionic crystals with a large variety of acids.^{15–21} Although the previously reported structures are centrosymmetric, we succeeded to crystallize the three noncentrosymmetric structures of triphenylguanidine salts with carboxylic acids, reported here.

* To whom correspondence should be addressed. E-mail: psidonio@pollux.fis.uc.pt.

[†]CEMDRX, Physics Department, University of Coimbra.

[‡]CFC, Physics Department, University of Coimbra.

[¶]Faculdade de Ciências da Universidade de Lisboa.

[§]Instituto Superior Técnico.

Although the triphenylguanidinium cation (TPG⁺) is not octupolar since it loses the three-fold rotational symmetry in the crystal,²² it would be expected that the magnitude of the octupolar irreducible component would be appreciable because of the presence of the guanidinium central fragment.

When the crystal structure of a compound is known, its nonlinear optical properties can be estimated assuming the additivity of the molecular hyperpolarizabilities according to the oriented gas model first employed by Chemla et al.²³ In this model, the macroscopic crystal susceptibilities are obtained by performing a tensor sum of the microscopic hyperpolarizabilities of the unit cell, and the effects of the surroundings are described by local field factors.

To the best of our knowledge, the oriented gas calculations reported in the literature are usually limited to the case of one- or two-dimensional molecular units, and they use the relations between microscopic and macroscopic lowest-order nonlinearities derived in the theoretical study by Zyss and Oudar.²⁴ In the case of chromophores with three-dimensional charge transfer or when the actual chromophore is a pair of ions, these relations cannot be used at all or may lead to severe errors. In these cases, the oriented gas calculations must be performed with the general expression. Also, most of the studies use the oriented gas approximation with the Lorenz–Lorentz local field correction.

In this study, we used a combination of the oriented gas model with the supermolecule approach, with the microscopic linear and nonlinear properties calculated by semiempirical methods. Several calculations using composite molecular species with different shapes and sizes are compared. We compare also the use of two different local field corrections, the anisotropic Lorenz–Lorentz spherical cavity local field factors and another approach by Wortmann and Bishop (W–B)²⁵ where an extension of the Onsager's reaction field model is used. The performance of the semiempirical methods PM3 and PM6 for the determination of polarizabilities and hyperpolarizabilities is also tested, by comparison with the experimental results.

2. Experimental and Computational Methods

2.1. Synthesis. Compound **1** (*N,N',N''*-triphenylguanidinium formate): 0.0102 g (0.0344 mmol) of *N,N',N''*-triphenylguanidine (TCI, 97%) was dissolved in 20 mL of ethanol, and 1 mL of formic acid (Sigma–Aldrich, ≥95%) was added to this solution. Additionally, 20 mL of water was added to the solution. The solution was stirred for 30 min at 40 °C and left to evaporate under ambient conditions. After 15 days, small prism-like yellowish single crystals with appropriate quality for X-ray measurements were deposited.

Compound **2** (*N,N',N''*-triphenylguanidinium benzoate): 0.0174 g (0.142 mmol) of benzoic acid (Sigma–Aldrich, ≥ 99.5%) was dissolved in 50 mL of boiling water, and 0.0421 (0.141 mmol) of *N,N',N''*-triphenylguanidine (TCI, 97%) was dissolved in 50 mL of boiling ethanol. The acid solution was slowly added to the basic solution. The resultant solution was then left to evaporate at room temperature and pressure. After 3 weeks, small single crystals, transparent and colorless, were obtained.

Compound **3** (*N,N',N''*-triphenylguanidinium *m*-methoxybenzoate): 0.0128 g (0.0833 mmol) of *m*-methoxybenzoic acid (Sigma–Aldrich, ≥ 99%) and 0.0247 (0.0834 mmol) of *N,N',N''*-triphenylguanidine (TCI, 97%) were dissolved in 100 mL of ethanol. After approximately 1 month, transparent single crystals with a thin plate habit appeared in the solution.

The crystals of TPG used in the Kurtz and Perry powder experiments were grown from an ethanolic solution of TPG (97%) purchased from TCI.

TABLE 1: Crystal Data and Structure Refinement of the *N,N',N''*-Triphenylguanidinium Salts^a

salt	1	2	3
emp. formula	C ₂₀ H ₁₉ N ₃ O ₂	C ₂₆ H ₂₃ N ₃ O ₂	C ₂₇ H ₂₅ N ₃ O ₂
formula weight	333.38	409.47	439.50
temperature (K)	293(2)	293(2)	293(2)
wavelength (Å)	0.71073	0.71073	0.71073
crystal system	orthorh.	monoc.	orthorh.
space group	<i>P</i> 2 ₁ 2 ₁ 2 ₁	<i>C</i> c	<i>P</i> 2 ₁ 2 ₁ 2 ₁
<i>a</i> (Å)	7.4214(2)	11.4369(15)	7.2482(2)
<i>b</i> (Å)	11.3585(4)	15.8900(18)	10.9828(3)
<i>c</i> (Å)	21.3888(7)	13.525(3)	29.0436(9)
α(°)	90	90	90
β(°)	90	113.170(11)	90
γ(°)	90	90	90
volume (Å ³)	1802.99(10)	2259.6(6)	2312.03(11)
<i>Z</i>	4	4	4
calc. dens. (g/cm ³)	1.228	1.204	1.263
abs. coef. (mm ⁻¹)	0.081	0.077	0.083
extinction coef.	0.059(5)	—	0.052(4)
<i>F</i> (000)	704	864	928
crystal size (mm)	0.37 × 0.12 × 0.09	0.30 × 0.14 × 0.08	0.38 × 0.11 × 0.03
data collec. range	1.90–27. 88°	2.32–27. 53°	1.98–26. 66°
index ranges: <i>h</i>	–8, 9	–14, 14	–8, 9
<i>k</i>	–13, 14	0, 20	–13, 13
<i>l</i>	–28, 28	–17, 6	–35, 34
Reflections:			
collected	57924	3951	61472
unique	2381	2601	2523
<i>R</i> (int)	0.0508	0.0154	0.0624
completeness (θ = 25.00°)	100%	100%	99.2%
refin. method		full-matrix least-squares	on <i>F</i> ²
data/restraints/parameters	2381/0/227	2601/2/280	2523/0/300
<i>F</i> ² goodness-of-fit	1.140	1.030	1.190
<i>R</i> indices:			
final [<i>I</i> > 2σ(<i>I</i>)]	0.0470	0.0370	0.0453
<i>wR</i> ₂	0.1036	0.0936	0.0974
all data	0.0912	0.0622	0.0847
<i>wR</i> ₂	0.1374	0.1070	0.1278
Largest diff. peak and hole (eÅ ⁻³)	0.482	0.123	0.409
	–0.497	–0.152	–0.360

^a **1**: *N, N', N''*-triphenylguanidinium formate; **2**: *N, N', N''*-triphenylguanidinium benzoate; **3**: *N, N', N''*-triphenylguanidinium *m*-methoxybenzoate.

2.2. X-ray Diffraction Studies. The diffraction measurements for *N, N', N''*-triphenylguanidinium benzoate were carried out on a single crystal using Mo Kα radiation on a CAD-4 diffractometer. Data reduction was performed with HELENA.²⁶ Lorenz and polarization corrections were applied. For the other two salts, the diffraction measurements were carried out on single crystals using Mo Kα radiation on a Bruker APEX II diffractometer.²⁷ Data reduction was performed with SMART and SAINT software.²⁷ Lorenz and polarization corrections were applied. Absorption correction was applied using SADABS. The structures were solved by direct methods using SHELXS-97 program²⁸ and refined on *F*²s by full-matrix least-squares with SHELXL-97 program.²⁸ The anisotropic displacement parameters for non-hydrogen atoms were applied. The hydrogen atoms were placed at calculated positions and refined with isotropic parameters as riding atoms. An extinction correction was applied during the refinements of the *N, N', N''*-triphenylguanidinium formate and *N, N', N''*-triphenylguanidinium *m*-methoxybenzoate structures.²⁸ The crystal data and details concerning data collection and structure refinement are given in Table 1.

Because of the weak anomalous scattering at the Mo wavelength, the absolute structures could not be determined from the X-ray data.

2.3. Kurtz and Perry Powder Method. The efficiency on SHG of the orthorhombic polymorph of TPG and of the reported TPG salts was measured using the Kurtz and Perry powder method.²⁹ The measurements were performed at the fundamental wavelength of 1064 nm originated directly by a Nd:YAG laser at low power (50 mJ per pulse), producing 40 ns pulses with a repetition rate of 10 Hz. The experimental setup is described in detail in ref 30. The second-harmonic light produced on the sample was collected by a spherical mirror and sent to the detector through two interference filters (for the second harmonic) in order to eliminate the fundamental laser light as well as any other light present in the sample. The detector used in the measurements of the efficiencies was a photomultiplier. The voltage from the photomultiplier was measured by the oscilloscope, which was triggered by the signal itself. The photomultiplier voltage and the neutral density filter area were optimized to obtain a good signal-to-noise relation and prevent the saturation of the photomultiplier. The oscilloscope measured the time integral of the photomultiplier voltage automatically, which was proportional to the SHG efficiency. The oscilloscope also performed, automatically, the average over several laser shots. In order to investigate the existence of phase matching, the intensity dependence on the particle size of TPG powder samples was studied. For these measurements, the detector used was a silicon photodiode (Thorlabs model DET100A/M) connected to an oscilloscope. The measurements taken in the oscilloscope were the pulse peak amplitude and the time integral of the pulse amplitude (pulse area). The oscilloscope was triggered by the signal itself. The measurements were taken from a single shot to an average of a few hundred shots depending on the compound resistance to intense laser light. Even at the single shot, an average of at least five shots was taken to reduce the error caused by laser power variation or thermal fluctuations. The SHG efficiency measurement of the urea reference sample was performed under the same experimental conditions as those of each test sample.

The samples preparation procedure was the following: the materials were milled to a fine powder and compacted in a mount and then installed in the sample holder. Sample grain sizes were not standardized. For this reason, signals between individual measurements were seen to vary in some cases by as much as $\pm 20\%$. For a proper comparison with the urea reference material, the measurements were averaged over several laser thermal cycles.

To investigate the existence of phase matching in TPG, one sample was ground to a fine powder and sieved into different particle size ranges (<63, 63–90, 90–125, 125–212, and 212–355 μm), compacted in a mount, and then installed in the sample holder. For a proper comparison with the urea reference material, the measurements were performed with urea sieved at the same grain size as the samples, averaged over several laser thermal cycles. The results of the efficiencies were obtained by the signal area ratio. Due to lack of sufficient material of the three salts, the investigation of the existence of phase matching was not performed for these samples.

2.4. Computational Methods. 2.4.1. Calculation of Microscopic Optical Properties. The static α and β tensor components used in the oriented gas model calculations were computed with the PM3^{31–34} and PM6³⁵ Hamiltonians available in MOPAC2009.³⁶ Several microscopic units ranging from the single molecule (or pair of ions) to clusters with different sizes and shapes were considered, with the ions' relative positions and geometries as those in the crystals (since the optimized structures were very different from those obtained with the X-ray

diffraction studies as the structure optimization performed in vacuum did not take into consideration all of the interactions of the crystalline environment).

2.4.2. Calculation of Macroscopic Optical Properties. In most organic molecular crystals, the energy of van der Waals or hydrogen bonds responsible for the intermolecular cohesion is much weaker, by 1 or 2 orders of magnitude, than that of intramolecular chemical bonds. Molecules remain therefore distinguishable entities, and the macroscopic nonlinear response of the materials may be described using a simple summation scheme following the oriented gas model, whereby the macroscopic second-order susceptibility tensor d_{IJK} originates essentially from the molecular quadratic hyperpolarizability tensor β_{ijk} expressed in molecular coordinates i, j, k .²⁴ The susceptibility coefficients depend on the crystal symmetry, the precise orientation of the molecule with respect to the crystal axes, and the conformation of the molecule. The relationship between microscopic and macroscopic parameters is given by

$$d_{IJK}(-\omega; \omega_1, \omega_2) = \frac{N}{V} f_I(\omega) f_J(\omega_1) f_K(\omega_2) b_{IJK}$$

$$b_{IJK} = \frac{1}{N_g} \sum_s \sum_{ijk} \cos \theta_{ii}^{(s)} \cos \theta_{jj}^{(s)} \cos \theta_{kk}^{(s)} \times \beta_{ijk}^{(s)}(-\omega; \omega_1, \omega_2) \quad (1)$$

where I, J, K are the crystal axes, N_g is the number of equivalent positions in the unit cell of volume V that has N molecules, $f_I(\omega)$ are local field factors appropriate for the crystal axis I , and the cosine product terms represent the rotation from the molecular reference frame onto the crystal frame. The equivalent positions are labeled by the index s . The local field factors are essentially a correction for the difference between an applied field that would be felt by the molecule in free space and the local field detected in a material, and according to Hamada,³⁷ the oriented gas approximation may be meaningless if it is used without this correction. Beyond the crudest approximation that consists of neglecting these local field factors altogether ($f_i = 1$), several expressions have been used to account for the anisotropy of the medium. The simplest is the anisotropic Lorenz–Lorentz spherical cavity expression

$$f_i(\omega) = \frac{(n_i(\omega)^2 + 2)}{3} = \frac{1}{1 - \frac{4}{3}\pi \frac{N}{V} a_{ii}} \quad (2)$$

where the refractive indices $n_i(\omega)$ are related, within the principal dielectric axis reference frame, to a diagonal tensor a_{ii} representing the average linear polarizability of the unit cell per molecule, which can be related, within the oriented gas model, to the molecular linear polarizability α_{ij} by

$$a_{ii} = \frac{1}{N_g} \sum_s \sum_{ij} \cos \theta_{ii}^{(s)} \cos \theta_{jj}^{(s)} \alpha_{ij}^{(s)} \quad (3)$$

It is important to recall that by using this expression for $f_i(\omega)$, one assumes that the nonlinear contribution to the local field is negligible. This relationship can be improved by considering an ellipsoidal cavity for which analytical expressions can be found from solving the Maxwell equations with boundary conditions.³⁸ However, there is evidence that the Lorenz–Lorentz (L–L) field factor, commonly used in extracting hyperpolarizabilities from experimental susceptibilities, may introduce errors of 50% or more.³⁹

Wortmann and Bishop (W–B)²⁵ addressed the problem of connecting single-molecule property calculations and actual measurements deriving local field factors from an extension of Onsager's reaction field model. Onsager⁴⁰ expressed the local field \mathbf{E}^L at the location of a solute molecule as the sum of the cavity field \mathbf{E}^C and the reaction field \mathbf{E}^R

$$\mathbf{E}^L = \mathbf{E}^C + \mathbf{E}^R \quad (4)$$

In the generalization of W–B to nonlinear optics, the local field is decomposed into Fourier components with amplitudes $\mathbf{E}^{L\Omega}$, $\mathbf{E}^{C\Omega}$, and $\mathbf{E}^{R\Omega}$

$$\mathbf{E}^{L\Omega} = \mathbf{E}^{C\Omega} + \mathbf{E}^{R\Omega} \quad (5)$$

and a local response of the medium to a uniform electric field is assumed. The cavity field is related to the macroscopic field in the medium by³⁸

$$\mathbf{E}^{C\Omega} = \mathbf{f}^{C\Omega} \cdot \mathbf{E}^\Omega \quad (6)$$

where $\mathbf{f}^{C\Omega}$ is the cavity field tensor at frequency Ω . The reaction field is related to the total (permanent + induced) dipole moment \mathbf{p}^Ω of the solute molecule at frequency Ω according to³⁸

$$\mathbf{E}^{R\Omega} = \mathbf{f}^{R\Omega} \cdot \mathbf{p}^\Omega \quad (7)$$

where $\mathbf{f}^{R\Omega}$ is the reaction field tensor.

The effective first-order hyperpolarizability $\beta_{\text{rst}}^{\text{eff}}(-2\omega; \omega, \omega)$ of the molecule in the cavity (solute molecule) $\beta_{\text{rst}}^{\text{sol}}(-2\omega; \omega, \omega)$ derived by W–B is given by

$$\beta_{\text{rst}}^{\text{eff}}(-2\omega; \omega, \omega) = F_{\text{rr}}^{\text{R}\omega} (F_{\text{ss}}^{\text{R}\omega} f_{\text{ss}}^{\text{C}\omega}) (F_{\text{tt}}^{\text{R}\omega} f_{\text{tt}}^{\text{C}\omega}) \times \beta_{\text{rst}}^{\text{sol}}(-2\omega; \omega, \omega) \quad (8)$$

where they used the argument that, to first order, the cavity field does not contain Fourier components at any harmonic frequencies. In eq 8, $F_{\text{rr}}^{\text{R}\omega}$ is related to the reaction field factor $f_{\text{rr}}^{\text{R}\omega}$ by

$$F_{\text{rr}}^{\text{R}\omega} = \frac{1}{1 - f_{\text{rr}}^{\text{R}\omega} \alpha_{\text{rr}}^{\text{sol}}(-\omega; \omega)} \quad (9)$$

where $\alpha_{\text{rr}}^{\text{sol}}(-\omega; \omega)$ is one diagonal component of the polarizability in the gas phase.

For an ellipsoidal cavity with semiaxes a_1, a_2, a_3 in a medium with dielectric constant ϵ^ω at frequency ω , the cavity and reaction field tensor components are given by³⁸

$$f_{\text{rs}}^{\text{C}\omega} = \frac{\epsilon^\omega}{\epsilon^\omega - \kappa_{\text{r}}(\epsilon^\omega - 1)} \delta_{rs} \quad (10)$$

$$f_{\text{rs}}^{\text{R}\omega} = \frac{3\kappa_{\text{r}}(1 - \kappa_{\text{r}})(\epsilon^\omega - 1)}{a_1 a_2 a_3 [\epsilon^\omega - \kappa_{\text{r}}(\epsilon^\omega - 1)]} \delta_{rs} \quad (11)$$

The quantities κ_{r} depend on the form of the ellipsoid and are given by³⁸

$$\kappa_{\text{r}} = \frac{a_1 a_2 a_3}{2} \int_0^\infty \frac{ds}{(s + a_{\text{r}}^2)[(s + a_1^2)(s + a_2^2)(s + a_3^2)]^{1/2}} \quad (12)$$

and they satisfy the relation $\kappa_1 + \kappa_2 + \kappa_3 = 1$.

The local field correction of eq 8, originally proposed in the context of solutions, can be used in eq 1 to relate the macroscopic second-order susceptibility tensor d_{IJK} to the unit cell nonlinearity per molecule b_{IJK} . When there are no experimental values of the refractive indices, the components of the dielectric constant tensor in the dielectric frame can be obtained from the calculated polarizability using the Onsager–Böttcher relation for an ellipsoidal cavity³⁸

$$\frac{12\pi\epsilon_{II}}{(\epsilon_{II} - 1)(2\epsilon_{II} + 1)} = \frac{V}{N} \frac{2 + x - 3\kappa_{\text{r}}x - \frac{9\kappa_{\text{r}}(1 - \kappa_{\text{r}}x)a_{II}}{a_1 a_2 a_3}}{2a_{II}} \quad (13)$$

where $x = 2(\epsilon_{II} - 1)/(2\epsilon_{II} + 1)$. The ellipsoidal cavity is adapted to the shape and dimensions of the clusters, and its volume obeys the condition $(4\pi/3)(N/V)a_1 a_2 a_3 = 1$. It should be noted that the semiaxes of the ellipsoidal cavity are aligned with the dielectric principal axes.

Regarding the dielectric reference frame ($\tilde{X}\tilde{Y}\tilde{Z}$) used in the calculations, it must be pointed out that, for the orthorhombic space groups, the dielectric axes are parallel to the crystallographic axes, but for the case of the lower-symmetry point group m (e.g., compound **2**), only the \tilde{Y} axis will coincide with the crystallographic [010] axis that is perpendicular to the glide planes, while the two other dielectric axes, which lie in the (010) plane, are free, in general, to rotate about the [010] axis depending on the light frequency. However, the specific molecular content of the unit cell can lock the dielectric axes to the crystallographic axes. The principal dielectric axes can be defined as the set of eigendirections of the crystalline polarizability tensor a_{IJ} if it is assumed that local field corrections will not introduce further rotations.⁴¹ The rotation Ψ around b of the principal dielectric axis \tilde{X} (or \tilde{Z}) away from the crystal axis a (or c , respectively) can be calculated from the diagonalization of the a_{IJ} tensor, which leads to the following expression

$$\tan(2\Psi) = \frac{2a_{XZ}}{a_{XX} - a_{ZZ}} \quad (14)$$

We calculated the unit cell nonlinearity per molecule, b_{IJK} , using the PM3- and PM6-calculated values of the microscopic quadratic polarizability β tensor components and taking into account the crystal symmetry of each material. The β_{ijk} values, for all crystals under consideration, were calculated in the molecular Cartesian coordinate system and then transformed into the crystal coordinate system with the aid of VMD code (version 1.8.6, April 7, 2007).⁴² The macroscopic NLO coefficients, d_{IJK} , were obtained using eq 1 with the L–L or the W–B local field factors. The local field factors were calculated using the average linear polarizability of the unit cell per molecule, a , which is related to the microscopic tensor α by the same rotation matrix as that obtained with VMD.

3. Results and Discussion

3.1. Crystal Structures. The three TPG salts crystallize in noncentrosymmetric space groups. Triphenylguanidinium for-

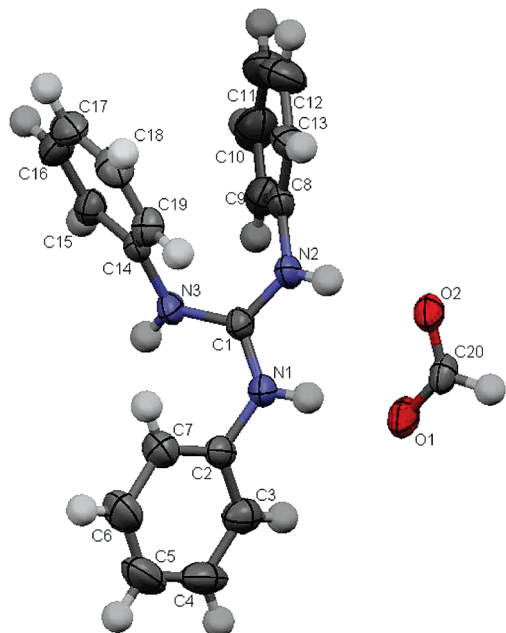


Figure 1. Molecular structure (thermal ellipsoids at 50% probability) and the atom numbering scheme for compound **1** (Mercury⁴³).

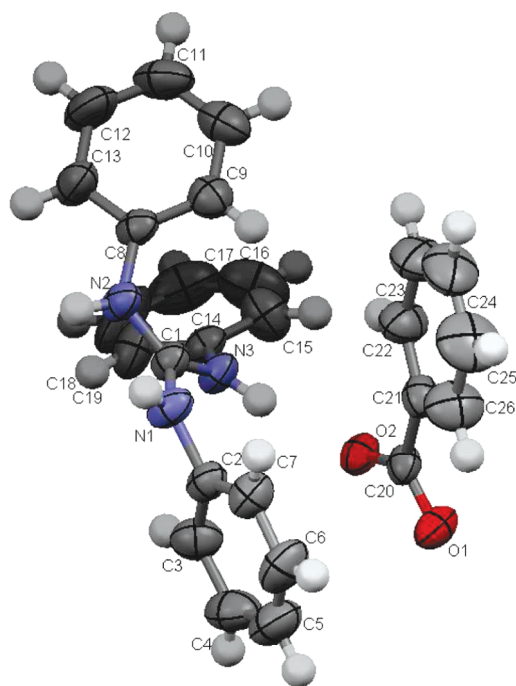


Figure 2. Molecular structure (thermal ellipsoids at 50% probability) and the atom numbering scheme for compound **2** (Mercury⁴³).

mate (Figure 1) and triphenylguanidinium *m*-methoxybenzoate (Figure 3) are orthorhombic with the chiral space group $P2_12_12_1$, while triphenylguanidinium benzoate (Figure 2) crystallizes in the monoclinic polar space group Cc . In all of these structures, the ions are assembled in chains by moderate to strong $N-H\cdots O$ hydrogen bonds.

Supplementary data have been deposited at the Cambridge Crystallographic Data Centre (CCDC No. 746265, No. 746266, and No. 746267). These data can be obtained free of charge from The Cambridge Crystallographic Data Centre via www.ccdc.cam.ac.uk/data_request/cif.

According to a search of the Cambridge Structural Database (CSD version 5.30, November 2008), triphenylguanidinium

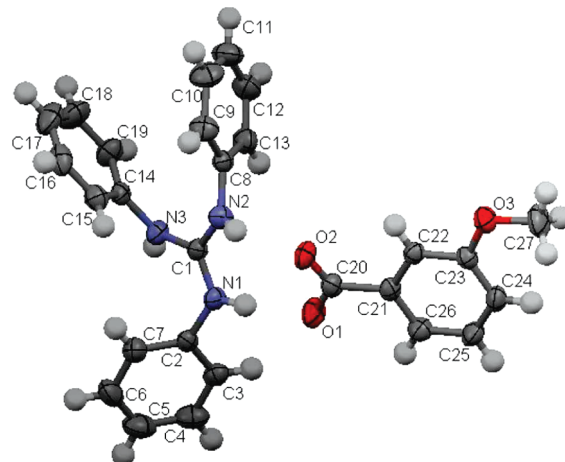


Figure 3. Molecular structure (thermal ellipsoids at 50% probability) and the atom numbering scheme for compound **3** (Mercury⁴³).

TABLE 2: Selected Structural Parameters (Å, °) of the Three Salts

	1	2	3
C1–N1	1.323(3)	1.317(3)	1.321(4)
C1–N2	1.332(3)	1.338(3)	1.333(4)
C1–N3	1.349(3)	1.342(3)	1.350(4)
N1–C2	1.420(3)	1.428(3)	1.421(4)
N2–C8	1.433(3)	1.418(3)	1.434(4)
N3–C14	1.421(3)	1.421(3)	1.423(4)
C20–O1	1.236(3)	1.247(3)	1.247(4)
C20–O2	1.237(3)	1.258(3)	1.267(4)
N1–C1–N2	117.6(2)	117.0(2)	118.5(3)
N1–C1–N3	121.8(2)	121.6(2)	120.8(3)
N2–C1–N3	120.6(2)	121.4(2)	120.7(2)
C1–N1–C2	127.3(2)	126.9(2)	125.8(3)
C1–N2–C8	123.6(2)	124.9(2)	123.5(3)
C1–N3–C14	122.7(2)	124.1(2)	123.6(3)
O1–C20–O2	127.7(2)	124.6(2)	124.9(3)
C2–N1–C1–N2	163.4(2)	168.5(3)	164.2(3)
C2–N1–C1–N3	–16.7(4)	–12.8(4)	–16.6(4)
C8–N2–C1–N1	155.4(2)	144.0(3)	152.5(3)
C8–N2–C1–N3	–24.5(4)	–34.7(4)	–26.7(4)
C14–N3–C1–N1	144.8(2)	157.7(2)	148.3(3)
C14–N3–C1–N2	–35.3(4)	–23.7(4)	–32.5(4)
C3–C2–N1–C1	146.9(3)	–51.1(4)	136.5(3)
C1–N2–C8–C13	128.5(3)	150.9(3)	–57.3(4)
C1–N3–C14–C19	–44.3(3)	–43.7(4)	131.5(3)

m-methoxybenzoate is the first crystal structure of a *m*-methoxybenzoic acid salt to be reported.

The CN_3 fragment of the guanidinium group of the N,N,N' -triphenylguanidinium cation has a planar geometry in the three salts, as expected for sp^2 hybridization of the central C atom, since the sum of the valence angles around C1 is $360.0(3)^\circ$, but the $N-C-N$ angles differ considerably from the mean value of 120° . The largest deviation is that of $N1-C1-N2$ in triphenylguanidinium benzoate [$117.0(2)^\circ$]. The bond lengths $C1-N$ are within the range expected for a delocalized $C-N$ bond (see Table 2).

The lengths of the $N-C(Ph)$ bonds (see Table 2) reveal more delocalization of the nitrogen lone pair electron density out onto the attached phenyl rings than that in neutral TPG.⁴⁴ In the three crystals, the C_{aryl} atoms are not coplanar with the guanidinium group, and inspection of the torsion angles shows that the twist angles around the $C1-N$ bonds differ for each ring (see Table 2). Also, the individual rotation angles of the phenyl rings around the $C_{aryl}-N$ bonds are different for each ring in the three structures. The angles between the least-squares planes of the

TABLE 3: Angles between the Least-Squares Planes of the Guanidinium Central Fragment and the Phenyl Rings (°)

ring	1	2	3
C2–C7	46.3(1)	57.7(1)	55.4(1)
C8–C13	67.2(1)	59.9(1)	73.5(1)
C14–C19	67.7(1)	57.7(1)	70.6(1)

guanidinium central fragment and the phenyl rings vary from 46.3(1) to 73.5(1)° (see Table 3), revealing the flexibility of the triphenylguanidinium cation.

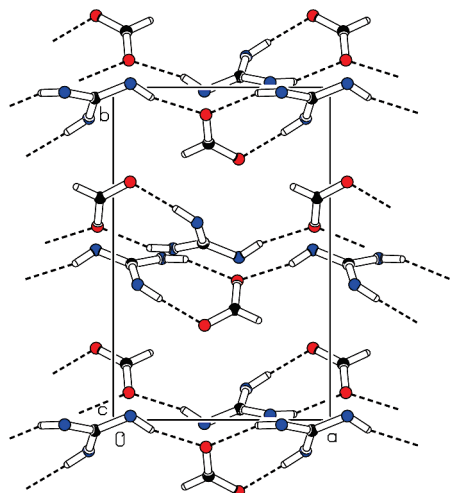
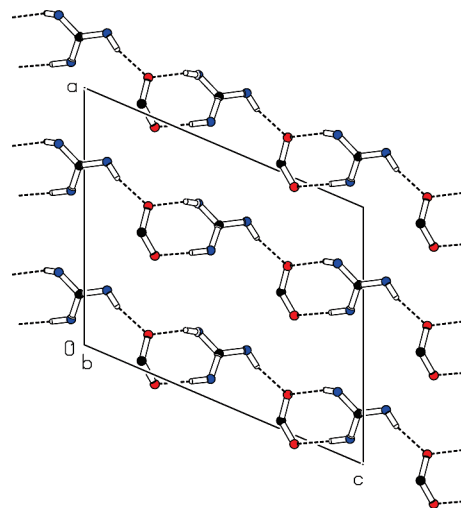
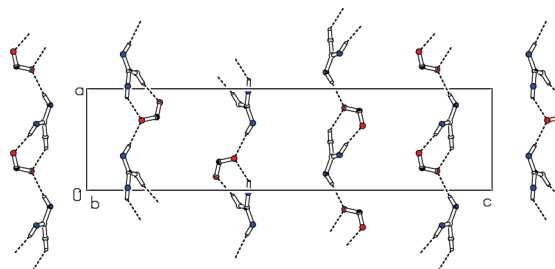
Regarding the anions of the three structures, the O–C–O angles of the carboxylate groups are greater than 120° because of the steric effect of lone pair electrons on both O atoms. The bond lengths in the deprotonated carboxyl groups are intermediate between normal single C_{sp²}–O (1.308–1.320 Å) and double C_{sp²}=O bond lengths (1.214–1.224 Å),⁴⁵ indicating delocalization of the charge over both O atoms of the COO[−] group.

In triphenylguanidinium benzoate, the carboxylate group of the anion is rotated 14.9(3)° out of the benzenic ring.

The carboxylate group of *m*-methoxybenzoate is bent out of the plane of the benzene ring by 4.7° and is also twisted approximately 14° around the C20–C21 bond. In the methoxy substituent, the O atom and the methyl C are almost exactly in the plane of the benzenic ring, with deviations of 0.011(4) and 0.028(6) Å, respectively.

Anions and cations are linked by intermolecular hydrogen bonds. Full hydrogen bond capability of the triphenylguanidinium cations is achieved in the three structures, every H atom being donated to an O atom of the carboxylate group of the respective anion. In each anion, the O1 atom accepts one H atom, while the O2 atom is an acceptor of two H atoms (Figures 4–6, Table 4). In the two salts with orthorhombic structures, the cations are linked in infinite chains running parallel to the *a* axis. The hydrogen-bonding functionality of the monoclinic structure is identical, but the infinite chains run along the *c* axis.

Graph-set analysis⁴⁶ shows that the hydrogen-bonding motifs are similar in the three salts (see Table 5). The main feature is the formation of rings of descriptor R₂²(8), according to Etter's graph-set theory.⁴⁶ Another salt of TPG with a carboxylic acid, namely, trifluoroacetic acid, has the same type of hydrogen bond topology.¹⁷ These conserved hydrogen-bonding motifs may serve as robust synthons in crystal engineering and design.⁴⁷ It could be expected that salts of TPG with other carboxylic acids will

**Figure 4.** Projection of the packing diagram of **1** along the *c* axis, with the hydrogen bonds depicted as dashed lines. The phenyl rings have been omitted for clarity.**Figure 5.** Projection of the packing diagram of **2** along the *b* axis, with the hydrogen bonds depicted as dashed lines. The benzenic rings have been omitted for clarity.**Figure 6.** Projection of the packing diagram of **3** along the *b* axis, with the hydrogen bonds depicted as dashed lines. Molecular fragments not involved in the hydrogen bonds have been omitted for clarity.**TABLE 4: Hydrogen-Bonding Geometry (Å, °) of the Reported Salts**

	D–H	H···A	D···A	D–H···A
1				
a N1–H1···O1	0.86	1.83	2.687(3)	174.8
b N2–H2···O2	0.86	2.04	2.868(3)	160.5
c N3–H3···O2 ^a	0.86	2.00	2.831(3)	163.0
2				
a N1–H1···O1 ^b	0.86	1.85	2.682(3)	162.6
b N2–H2···O2 ^b	0.86	1.95	2.764(3)	157.4
c N3–H3···O2	0.86	1.97	2.813(3)	164.7
3				
a N1–H1···O1	0.86	1.82	2.667(3)	168.8
b N2–H2···O2	0.86	2.05	2.794(3)	144.5
c N3–H3···O2 ^c	0.86	2.07	2.920(3)	168.5

^a Symmetry code: $x - 1, y, z$. ^b Symmetry code: $x, -y, z - 1/2$. ^c Symmetry code: $x + 1, y, z$.

crystallize with the same hydrogen bond pattern, unless the acids have other hydrogen acceptors that compete with the carboxylate group.

3.2. Kurtz and Perry Powder Method Results. The powder SHG technique of Kurtz and Perry²⁹ still plays an important role as a method for fast initial screening of noncentrosymmetric structures, although more elaborate methods are being developed.^{48–50} The Kurtz and Perry method can give some qualitative measure of the second-harmonic efficiency to assess whether a material may be useful for the purpose of nonlinear optics.⁵¹ The results of the Kurtz and Perry powder tests are presented in Table 6.

The interpretation of the powder SHG data is not simple, and the results must be taken with caution. It is clear that for

TABLE 5: Graph-Set Descriptors of the Motifs and Second-Order Networks Involving the Hydrogen Bonds of Table 4

	a	b	c
a	D	R ₂ ² (8)	C ₂ ² (8)
b		D	C ₂ ² (6)
c			D

TABLE 6: SHG Efficiencies Compared to the Urea Standard

	compound			
	TPG	1	2	3
SHG efficiency	0.8	0.02	0.18	~0.01

TABLE 7: SHG Efficiencies of TPG for Different Particle Sizes Compared to the Urea Standard

particle sizes (μm)	SHG intensity	error
<63	0.62	3%
63–90	0.60	3%
90–125	4.70	6%
125–212	0.71	6%
212–355	1.34	6%

any quantitative comparison, one should take into account properties of the particular experimental arrangement like particle size and index-matching conditions. Nonetheless, it is possible to conclude that TPG is appreciably more efficient than the three salts studied.

Using this technique, it is also possible to determine the existence of phase matching in new materials. In a nonphase-matching material, the maximum intensity is achieved when the particle size approximately matches the average coherence length and then falls with any increase in particle size. In a phase-matching material the intensity, in contrast, reaches a plateau at large particle sizes. An alternative technique would be the use of a tunable laser source, as proposed by Tang,⁵² that determines the limits of the spectral range over which phase matching can be achieved.

In order to investigate the existence of phase matching in TPG, the intensity dependence on particle size was monitored. It is clear from the results of Table 7 that TPG is a nonphase-matchable material. Although the intensity does not diminish consistently throughout the samples prepared with larger and larger particles, this is probably due to imperfect filtering allowing smaller particles to remain in the larger particle samples. The highest intensity recorded gave an estimated SHG efficiency of 4.7 times that of urea, giving an estimated average effective nonlinearity of around 2 times that of urea. However, nonphase-matchability has a damping down effect in this technique, and therefore, in such a case, the true value of the average effective nonlinearity could be significantly larger.

3.3. Calculated Nonlinear Optical Properties. In this section, we present the macroscopic NLO coefficients, d_{ijk} , calculated from the molecular quadratic hyperpolarizability tensor β_{ijk} with the methodology described in section 2.4.2. The calculations were performed for the three salts and for the free base. The shapes of the clusters used in the calculations were chosen in such a way as to take into account the strongest intermolecular interactions.

Using the crystal structure of TPG taken from ref 44, we calculated the β_{ijk} tensor components for the isolated molecule, for chains along the a axis with 2, 3, 4, 5, and 6 molecules (here called 1c2m, 1c3m, 1c4m, 1c5m, and 1c6m, respectively), and also for clusters with two neighboring chains of 2, 3, and

TABLE 8: Theoretical Susceptibility Components (pm/V) for TPG, Calculated from the β_{ijk} Components of the Isolated Molecule, for Chains along the a Axis with 2, 3, 4, 5, and 6 Molecules (here called, 1c2m, 1c3m, 1c4m, 1c5m, and 1c6m, respectively) and for Clusters with Two Neighboring Chains of 2, 3, and 4 Molecules (here called 2c2m, 2c3m and 2c4m, respectively): Lorenz–Lorentz Local Field Factors

	PM3				PM6			
	d_{zxx}	d_{zyy}	d_{zzz}	$\langle d \rangle$	d_{zxx}	d_{zyy}	d_{zzz}	$\langle d \rangle$
1 molecule	-9.8	21.4	12.5	15.1	-7.3	17.8	11.4	12.7
1c2m	-11.6	18.1	12.0	13.3	-8.7	14.5	9.8	10.6
1c3m	-13.3	15.2	10.8	12.0	-9.7	12.3	8.4	9.4
1c4m	-14.5	13.9	10.0	11.7	-10.5	11.2	7.7	9.0
1c5m	-15.2	13.1	9.2	11.5	-11.0	10.5	7.1	8.8
1c6m	-15.9	12.5	8.9	9.7	-11.4	10.1	6.8	8.7
2c2m	-12.1	17.7	12.0	13.2	-8.8	14.4	10.4	10.7
2c3m	-13.3	15.5	11.5	12.3	-9.6	12.4	9.6	9.7
2c4m	-13.9	14.6	10.6	11.9	-10.1	11.5	8.8	9.2

TABLE 9: Theoretical Susceptibility Components (pm/V) for TPG, Calculated from the β_{ijk} Components of the Isolated Molecule, for Chains along the a Axis with 2, 3, 4, 5, and 6 Molecules (here called 1c2m, 1c3m, 1c4m, 1c5m, and 1c6m, respectively) and for Clusters with Two Neighboring Chains of 2, 3, and 4 Molecules (here called 2c2m, 2c3m, and 2c4m, respectively): Wortmann–Bishop Local Field Factors

	PM3				PM6			
	d_{zxx}	d_{zyy}	d_{zzz}	$\langle d \rangle$	d_{zxx}	d_{zyy}	d_{zzz}	$\langle d \rangle$
1 molecule	-10.8	13.4	8.8	10.3	-7.6	11.1	8.0	8.4
1c2m	-9.0	13.4	10.7	10.3	-6.8	10.8	8.7	8.3
1c3m	-7.9	13.8	11.9	10.7	-5.9	11.2	9.0	8.4
1c4m	-7.6	14.5	12.8	11.2	-5.7	11.6	9.3	8.7
1c5m	-7.6	15.6	13.4	12.0	-5.7	12.3	9.6	9.2
1c6m	-7.6	16.3	14.4	12.6	-5.6	12.8	9.9	9.5
2c2m	-11.8	13.5	7.5	10.4	-8.3	11.0	6.5	8.2
2c3m	-9.4	15.7	8.7	11.1	-6.9	12.4	7.4	8.8
2c4m	-8.4	16.3	9.1	11.4	-6.3	12.6	7.6	8.9

4 molecules (here called 2c2m, 2c3m, and 2c4m, respectively). This crystal is orthorhombic with space group $Pna2_1$ and point group $mm2$; therefore, the only nonvanishing independent components of the second-order polarizability tensor allowed by this point group and by the Kleinman symmetry are d_{zxx} , d_{zyy} , and d_{zzz} .^{53,54} The results obtained with the L–L and the W–B local field corrections are presented in Tables 8 and 9, respectively. Along with the d_{ijk} components we also present the angular average of the NLO susceptibility, $\langle d^{2\omega} \rangle$, using the expression deduced by Kurtz and Perry.²⁹

The calculations for the salts were performed considering the following clusters: the closest ion pairs in which the carboxylate group participates in two hydrogen bonds with the guanidinium group (cluster1), a cluster of two chains of two dimers (cluster2), and a chain of four dimers (cluster3). The results of these calculations are presented in Tables 10 and 11.

By the $222-D_2$ symmetry and the Kleinman symmetry, there is only one nonvanishing independent component of the second-order polarizability tensor for the formate and m -methoxybenzoate salts, that is, d_{xyz} . For the benzoate salt (point group $m-C_{1h}$), the nonvanishing components of the susceptibility tensor are indicated in Tables 10 and 11.

Comparing several calculations, we can see that the PM3 Hamiltonian gives systematically higher values for the components of the second-order polarizability tensor. The comparison of the two local field corrections indicates that the calculations

TABLE 10: Theoretical Susceptibility Components (pm/V) for the TPG Salts Calculated from β_{ijk} Components of Several Clusters^a: Wortmann–Bishop Local Field Factors

		PM3			PM6		
		cluster1	cluster2	cluster3	cluster1	cluster2	cluster3
1	d_{xyz}	-3.4	0.6	-0.9	-1.4	0.9	-0.5
	$\langle d \rangle$	2.9	0.5	0.8	1.2	0.7	0.4
2	d_{xxx}	-23.6	-27.2	-7.3	-15.3	-21.1	-10.7
	d_{xyy}	-11.3	-10.5	-4.9	-7.2	-8.4	-6.7
	d_{xzz}	10.7	6.3	3.9	8.4	4.6	3.7
	d_{zxx}	-12.7	-10.0	-10.2	-13.1	-7.3	-11.6
	d_{zyy}	-8.4	0.9	-0.9	-5.2	0.8	-0.7
	d_{zzz}	-20.5	3.3	0.2	-10.5	3.3	1.9
$\langle d \rangle$		20.7	15.3	8.3	14.9	11.8	10.0
	d_{xyz}	-0.3	-0.8	-0.4	-0.5	-0.4	-0.3
$\langle d \rangle$		0.2	0.7	0.3	0.4	0.4	0.3

^a Cluster1: the closest ion pairs in which the carboxylate group participates in two hydrogen bonds with the guanidinium group; cluster2: two chains of two dimers; cluster3: chain of four dimers.

TABLE 11: Theoretical susceptibility components (pm/V) for the TPG salts calculated from the β_{ijk} components of several clusters (^a) - Wortmann-Bishop local-field factors

		PM3			PM6		
		cluster1	cluster2	cluster3	cluster1	cluster2	cluster3
1	d_{xyz}	-2.7	0.5	-1.0	-1.1	0.8	-0.6
	$\langle d \rangle$	2.3	0.5	0.8	0.9	0.7	0.5
2	d_{xxx}	-20.0	-17.3	-7.9	-13.0	-13.7	-13.1
	d_{xyy}	-8.9	-6.2	-5.2	-5.7	-5.1	-8.4
	d_{xzz}	8.2	5.9	2.4	6.4	4.2	2.0
	d_{zxx}	-11.1	-7.2	-10.7	-11.4	-5.3	-12.5
	d_{zyy}	-6.7	0.6	-0.9	-4.2	0.5	-0.8
	d_{zzz}	-16.2	3.4	0.1	-8.3	3.4	0.9
$\langle d \rangle$		17.0	9.8	8.6	12.4	7.7	11.6
	d_{xyz}	-0.2	-0.7	-0.4	-0.4	-0.4	-0.3
$\langle d \rangle$		0.2	0.6	0.3	0.3	0.3	0.3

^a Cluster1: the closest ion pairs in which the carboxylate group participates in two hydrogen bonds with the guanidinium group; cluster2: two chains of two dimers; cluster3: chain of four dimers.

using the Lorenz–Lorentz factors yield generally higher susceptibility components.

The calculations for TPG, although overestimating the experimental result, predict the correct order of magnitude of the SHG response (compare with the susceptibility of urea of 2.3 pm/V; see Appendix I of ref 55). This overestimation can be partially explained by the nonphase-matchability of the material. It can be seen, by comparing Tables 10 and 11, that the differences between the values of the susceptibility components calculated with different clusters are smaller using the W–B local field correction. Overall, the best results are obtained with PM6 Hamiltonian and W–B local field factors.

For the two orthorhombic salts (**1** and **3**), the calculations foresee poor results, and apparently, there is good agreement with the experimental values, but we cannot draw a definitive conclusion since the phase matching was not tested for these two materials. The results obtained with the different methods are quite similar for these salts, with the exception of PM3 calculations for the cluster1 of **1**, which overestimate the results.

The calculations for **2** show, by far, the worst disagreement with experiment. However, it seems that, once again, the best result is obtained with the cluster with more intermolecular interactions with the PM6 method and W–B local field correction.

To verify the reliability of our calculations, the same types of calculations were performed for two salts 2-amino-5-nitropyridinium dihydrogen phosphate (2A5NPDP), whose

TABLE 12: Calculated Susceptibility Components (pm/V) for 2A5NPDP Compared with the Experimental and Theoretical Values from Kotler et al.^{56,a}

	d_{15}	d_{24}	d_{33}	
dimer (PM3)	25.3	3.7	56.0	
(PM6)	14.0	-3.6	59.1	
chain2 (PM3)	19.6	2.4	46.1	L–L
(PM6)	10.9	-4.3	47.3	
2chains2 (PM3)	23.2	17.1	38.5	
(PM6)	13.1	4.3	40.2	
dimer (PM3)	19.8	3.2	38.0	
(PM6)	10.4	-3.2	36.2	
chain2 (PM3)	19.3	1.5	37.4	W–B
(PM6)	10.9	-2.3	37.7	
2chains2 (PM3)	19.2	12.1	33.0	
(PM6)	10.7	2.8	34.4	
theory ⁵⁶	28 ± 4	12 ± 1	87 ± 4	
$\lambda_{\text{fund}} = 1.34 \mu\text{m}$				
experiment ⁵⁶	6 ± 1		12 ± 1	
theory ⁵⁶	35 ± 1	16 ± 1	122 ± 4	
$\lambda_{\text{fund}} = 1.06 \mu\text{m}$				
experiment ⁵⁶	7 ± 1	1 ± 0.4		

^a The β_{ijk} components were calculated for the following clusters: a pair of ions (dimer), a chain of two pairs (chain2), and two chains of two pairs (2chains2).

crystal nonlinear coefficients were determined by the Maker fringe method at the fundamental wavelengths, 1.34 and 1.06 μm ,⁵⁶ and 2-amino-5-nitropyridinium chloride (2A5NPCl), with coefficients d_{12} , d_{13} , and d_{14} measured by phase-matched second-harmonic generation at 1.32 μm ⁵⁷ and coefficient d_{11} determined by the Maker fringe method at 1.32 μm .⁵⁸ For 2A5NPDP, we used the atomic coordinates determined by Masse and Zyss.⁵⁹ The crystal is orthorhombic with space group $Pna2_1$ (class $mm2$), and the unit cell parameters are $a = 25.645(8) \text{ \AA}$, $b = 6.228(2) \text{ \AA}$, and $c = 5.675(2) \text{ \AA}$. The atomic coordinates used in the calculations for 2A5NPCl were taken from the study by Pécaut et al.⁶⁰ The crystal structure of 2A5NPCl belongs to the monoclinic system (space group $P2_1$), and the lattice parameters are $a = 9.956(5) \text{ \AA}$, $b = 7.373(2) \text{ \AA}$, $c = 4.813(1) \text{ \AA}$, and $\beta = 95.86(6)^\circ$.

The results of the calculations for 2A5NPDP are presented in Table 12 for a pair of ions (dimer), for a chain of two pairs (chain2), and for two chains of two pairs (2chains2). The clusters used in the calculations for 2A5NPCl were the following: a pair of ions (dimer), a chain of two pairs (chain2), a chain of four pairs (chain4), two chains of two pairs (2chains2), and two chains of four pairs (2chains4). In the clusters 2chains2 and 2chains4, the zigzag chains belong to consecutive planes (201) containing the aromatic rings. The results of the calculations for 2A5NPCl are presented in Table 13. The theoretical values reported by Horiuchi et al.,⁵⁸ presented here for comparison, were calculated from the hyperpolarizabilities of the neutral 2-amino-5-nitropyridine molecule (2A5NP), the cation (2A5NP⁺), and the pair of ions (2A5NP⁺Cl⁻).

Our theoretical results for 2A5NPDP give a reasonable estimate of the crystalline NLO coefficients, and the best result corresponds to the calculation with one cluster of two chains, each chain with two ion pairs, using the PM6 Hamiltonian and the W–B local field correction. The calculations give systematically higher values, and the worst disagreement corresponds to the component d_{33} . This may be related to the fact that the dipoles of the 2-amino-5-nitropyridinium ions are aligned along the c axis so that most of the charge transfer will occur in this direction.

The d components calculated for 2A5NPDP are closer to the experimental values than the theoretical values obtained by

TABLE 13: Calculated Susceptibility Components (pm/V) for 2A5NPCL Compared with the Experimental and Theoretical Values from Horiuchi et al.^{58a}

	L-L				W-B			
	d_{11}	d_{12}	d_{13}	d_{14}	d_{11}	d_{12}	d_{13}	d_{14}
dimer (PM3)	-22.3	-22.8	-2.4	11.1	-9.0	-9.6	-2.7	7.6
(PM6)	-26.7	-43.8	-0.2	7.6	-9.5	-14.5	-0.2	-4.1
chain2 (PM3)	-20.2	-22.0	-0.1	-7.3	-7.8	-7.9	-0.1	-4.8
(PM6)	-28.3	-33.2	-0.3	-6.0	-9.2	-9.7	-0.2	-3.1
chain4 (PM3)	-23.7	-24.6	1.0	-6.4	-7.2	-8.2	1.2	-4.0
(PM6)	-42.6	-35.4	-0.4	-7.0	-9.7	-9.4	-0.3	-3.3
2chains2 (PM3)	-13.4	-19.8	1.7	-1.7	-9.1	-9.2	1.6	-1.1
(PM6)	-14.4	-22.6	0.3	-4.2	-7.4	-9.2	0.2	-2.5
2chains4 (PM3)	-10.9	-20.4	2.2	0.0	-4.1	-10.6	2.1	0.0
(PM6)	-19.1	-23.7	0.2	-5.0	-5.8	-10.0	0.2	-2.9
theory 2A5NP ⁵⁸	76.6	20.8	2.6	4.6				
theory 2A 5NP ⁺⁵⁸	28.8	3.4	0.9	0.0				
theory 2A 5NP ^{+ Cl⁻⁵⁸}	109.8	46.9	4.6	13.7				
experiment ^{57,58}	9 ± 4	8 ± 3	11 ± 4	~0				
$\lambda_{\text{fund}} = 1.32 \mu\text{m}$								

^a The β_{ijk} components were calculated for the following clusters: a pair of ions (dimer), a chain of two pairs (chain2), a chain of four pairs (chain4), two chains of two pairs (2chains2), and two chains of four pairs (2chains4).

TABLE 14: Calculated Refractive Indices for 2A5NPDP Compared with the Experimental Values at 1340 nm⁵⁶ (see text for details)

	PM3			PM6			
	n_x	n_y	n_z	n_x	n_y	d_z	
dimer	1.496	1.482	1.620	1.576	1.657	1.817	
chain2	1.500	1.451	1.647	1.559	1.686	1.789	L-L
2chains2	1.442	1.532	1.629	1.555	1.709	1.773	
dimer	1.498	1.508	1.638	1.580	1.707	1.841	
chain2	1.549	1.409	1.591	1.621	1.592	1.710	O-B
2chains2	1.448	1.505	1.607	1.564	1.661	1.743	
experimental ⁵⁶	1.581	1.613	1.681				

TABLE 15: Calculated Refractive Indices for 2A5NPCL Compared with the Experimental Values at 1320 nm⁵⁷ (see text for details)

	PM3			PM6			
	n_x	n_y	n_z	n_x	n_y	d_z	
dimer	1.751	1.636	1.516	1.869	1.823	1.308	
chain2	1.719	1.659	1.514	1.845	1.799	1.298	
chain4	1.733	1.651	1.519	1.903	1.771	1.297	L-L
2chains2	1.803	1.726	1.374	1.811	1.799	1.264	
2chains4	1.722	1.705	1.461	1.839	1.762	1.288	
dimer	1.610	1.522	1.467	1.687	1.613	1.288	
chain2	1.573	1.508	1.451	1.648	1.585	1.275	
chain4	1.541	1.497	1.414	1.625	1.563	1.265	O-B
2chains2	1.772	1.600	1.373	1.717	1.640	1.257	
2chains4	1.571	1.636	1.416	1.630	1.650	1.266	
experimental ⁵⁷	1.645	1.787	1.469				

Kotler et al.⁵⁶ The reasons invoked in ref 56 to account for the discrepancy between measured and calculated values were the following: (1) The hyperpolarizability of the neutral molecule has been used; (2) a one-dimensional model has been considered; (3) the molecular nonlinearity was corrected with L-L local field factors; and (4) the contribution of the phosphate anionic sublattice was neglected. All of these issues are addressed in our calculations.

Our calculations of the quadratic coefficients for 2A5NPCL show also a better performance of the W-B local field correction and of the larger clusters. However, in this particular case, it is more difficult to draw a definite conclusion about the best Hamiltonian.

The refractive indices were calculated from the L-L local field factors using eq 2 and from the square root of the

TABLE 16: Relation of the Ratio between Septor and Vector Scalar Invariants (ρ) with the HOMA Aromaticity Index and the Dipole Moment (the PM6 calculation referred to the ion's center of mass) for the TPG Molecule and TPG⁺ Ions of the Reported Salts

compound	μ (D)	HOMA	ρ
TPG	3.392	0.891	1.137
TPG ⁺ (1)	2.541	0.990	2.644
TPG ⁺ (3)	2.481	0.991	3.032
TPG ⁺ (2)	2.370	0.995	4.618

components of the dielectric constant tensor in the dielectric frame, obtained with eq 13, the Onsager-Böttcher (O-B) relation for an ellipsoidal cavity, using the calculated linear polarizability of the unit cell per molecule. All of these calculations were performed with the clusters indicated above. Kotler et al.⁵⁶ measured the refractive indices of 2A5NPDP at various wavelengths in the range of 468–1340 nm, and Horiuchi et al.⁵⁷ measured the refractive indices of 2A5NPCL in the 447–1320 nm range. Since our semiempirical calculations are static, we compare our results with the experimental refractive indices measured at the highest wavelengths (1340 nm for 2A5NPDP and 1320 nm for 2A5NPCL) (see Tables 14 and 15).

Once more, the best results are obtained with the larger clusters and using the O-B relation to extract the components of the dielectric constant tensor. For 2A5NPCL, only the larger cluster (2chains4) reproduces the correct order of the refractive indices ($n_y > n_x > n_z$), with the agreement with the experimental values being worse than that for 2A5NP.

3.3.1. Scalar Invariants of the Hyperpolarizability. The first hyperpolarizability β , being a fully symmetric third-rank tensor under Kleinmann symmetry, can be decomposed into two tensorial components $\beta_{J=1}$ and $\beta_{J=3}$, called, respectively, the dipolar (vector) and the octupolar (septor) irreducible components^{10,61}

$$\beta = \beta_{J=1} \oplus \beta_{J=3} \quad (15)$$

It was recognized by Jerphagnon⁶¹ that it is more useful to compare proper scalar invariants, related to this decomposition, than to compare the individual tensor components.

For the compounds studied, a considerable octupolar contribution to the NLO effect due to the guanidine and guanidinium fragments in TPG and TPG⁺, respectively, is expected. Using

the calculated values of the β components, it is possible to estimate the ratio ρ of the scalar invariants associated with the septor and the vector parts¹⁰

$$\rho = \frac{\|\beta_{J=3}\|}{\|\beta_{J=1}\|} \quad (16)$$

In the case of molecules with no particular symmetry, the most general formulas, corresponding to class 1, must be used to calculate the invariants.⁶²

We calculated the ρ values for TPG, TPG⁺, the chromophoric units of the salts (ion pairs), and also the unit cells when the crystalline symmetry allowed the existence of both components. All tensor components were taken from the PM6 calculations, and for the unit cell, we used the d components of the calculation with the largest cluster and W–B local field correction.

The vector part of the β tensor can be related to the dipole moment,⁶³ and the octupolar part will be higher for a system with trigonal symmetry; therefore, it is interesting to relate the ρ values of the TPG molecule and the TPG⁺ ions in the three salts with the dipole moment and the geometry of the central CN₃ fragments. We applied the geometry-based HOMA (harmonic oscillator measure of aromaticity) index of aromaticity^{64,65} (HOMA is defined to give 0 for a model nonaromatic system and 1 for a system where full π -electron delocalization occurs) to quantify the so-called Y aromaticity⁶⁶ of the guanidine and guanidinium fragments (see Table 16). The cations are more octupolar than TPG since the guanidinium core is more symmetric, which is reflected in the higher values of the HOMA index of the cations.

For crystals belonging to point group 222 (ex. space group $P2_12_12_1$), the d tensor reduces to a purely octupolar component, and its vector part is identically 0; therefore, only the octupolar part of the molecular β tensor will contribute to the crystalline d tensor. Since in TPG⁺ formate ($\rho = 0.774$) and TPG⁺ *m*-methoxybenzoate ($\rho = 0.846$), the octupolar part is appreciable but not dominant at the molecular level (with the ion pair as the chromophoric unit), most of this nonlinear response will not contribute to the macroscopic response. In TPG⁺ benzoate (class *m*), $\rho = 0.771$ at the molecular level and 1.151 for the unit cell. The TPG crystal may have both dipolar and octupolar contributions to the macroscopic second-order polarizability since it is a medium with *mm2* point symmetry. The TPG molecule has a slight predominance of the octupolar component of β ($\rho = 1.137$), and this component is also dominant in tensor d ($\rho = 1.662$).

4. Conclusions

In this paper, we have performed the calculation of the second-order susceptibility for crystals made of microscopic units with no special symmetry. The calculations were based on the oriented gas model in its most general formulation. We considered several types of microscopic units from the molecule to clusters of different sizes/shapes. We also used different local field corrections. For the calculation of the microscopic β tensor components, we used the semiempirical PM3 and PM6 Hamiltonians.

Comparison with the experimental data showed that consideration of a large cluster as the microscopic unit yields better theoretical results. Also, the use of the W–B local field factors instead of the usual L–L correction further improved the calculated d components. The PM6 Hamiltonian performed better in comparison with the older PM3.

We plan to apply this methodology (oriented gas model, large cluster, W–B local field correction, PM6 Hamiltonian) to more compounds with d components determined in accurate experiments.

Acknowledgment. This work was supported by Fundação para a Ciência e a Tecnologia (FCT), under the Scholarship SFRH/BD/38387/2008 and under the Project PTDC/FIS/103587/2008.

References and Notes

- (1) *Nonlinear Optical Properties of Organic Molecules and Crystals*; Chemla, D. S.; Zyss, J., Eds.; Academic Press: Orlando, FL, 1987; Vol. 1.
- (2) *Molecular Nonlinear Optics. Materials, Physics, and Devices*; Zyss, J., Ed.; Academic Press: Boston, MA, 1994.
- (3) Marder, S. R.; Perry, J. W.; Schaefer, W. P. *Science* **1989**, *245*, 626.
- (4) Lacroix, P. J.; Clément, R.; Nakatani, K.; Zyss, J.; Ledoux, I. *Science* **1994**, *263*, 658.
- (5) Pan, F.; Knöpfle, G.; Bosshard, C.; Follonier, S.; Spreiter, R.; Wong, M. S.; Günter, P. *Appl. Phys. Lett.* **1996**, *69*, 13.
- (6) Zyss, J.; Nicoud, J. F.; Coquillay, M. *J. Chem. Phys.* **1984**, *81*, 4160.
- (7) Josse, D.; Dou, S. X.; Zyss, J.; Andreazza, P.; Périgaud, A. *Appl. Phys. Lett.* **1992**, *61*, 121.
- (8) Oudar, J. L.; Zyss, J. *Phys. Rev. A* **1982**, *26*, 2016.
- (9) Zyss, J. *Nonlinear Opt.* **1991**, *1*, 3.
- (10) Zyss, J. *J. Chem. Phys.* **1993**, *98*, 6583.
- (11) Zyss, J.; Brasselet, S.; Thalladi, V. R.; Desiraju, G. R. *J. Chem. Phys.* **1998**, *109*, 658.
- (12) Zyss, J.; Ledoux-Rak, I.; Weiss, H.-C.; Bläser, D.; Boese, R.; Thallapally, P. K.; Thalladi, V. R.; Desiraju, G. R. *Chem. Mater.* **2003**, *15*, 3063.
- (13) Le Floch, V.; Brasselet, S.; Zyss, J.; Cho, B. R.; Lee, S. H.; Jeon, S.-J.; Cho, M.; Min, K. S.; Suh, M. P. *Adv. Mater.* **2005**, *17*, 196.
- (14) Zyss, J.; Pécaut, J.; Levy, J. P.; Masse, R. *Acta Crystallogr., Sect. B* **1993**, *49*, 334.
- (15) Kemme, A.; Rutkis, M.; Eiduss, J. *Latv. PSR Zinat. Akad. Vestis Kim. Ser.* **1988**, *5*, 595.
- (16) Pereira Silva, P. S.; Paixão, J. A.; Ramos Silva, M.; Matos Beja, A. *Acta Crystallogr., Sect. E* **2006**, *62*, o3073.
- (17) Pereira Silva, P. S.; Cardoso, C.; Ramos Silva, M.; Paixão, J. A. *Acta Crystallogr., Sect. E* **2007**, *63*, o501.
- (18) Pereira Silva, P. S.; Ramos Silva, M.; Paixão, J. A.; Matos Beja, A. *Acta Crystallogr., Sect. E* **2007**, *63*, o2243.
- (19) Pereira Silva, P. S.; Ramos Silva, M.; Paixão, J. A.; Matos Beja, A. *Acta Crystallogr., Sect. E* **2007**, *63*, o2524.
- (20) Dastychova, L.; Prihoda, J.; J., T. *Collect. Czech. Chem. Commun.* **2007**, *72*, 297.
- (21) Pereira Silva, P. S.; Domingos, S. R.; Ramos Silva, M.; Paixão, J. A.; Matos Beja, A. *Acta Crystallogr., Sect. E* **2008**, *64*, o1082.
- (22) Cardoso, C.; Pereira Silva, P. S.; Ramos Silva, M.; Matos Beja, A.; Paixão, J. A.; Nogueira, F.; Sobral, A. J. F. N. *J. Mol. Struct.* **2008**, *878*, 169.
- (23) Chemla, D. S.; Oudar, J. L.; Jerphagnon, J. *Phys. Rev. B* **1975**, *12*, 4534.
- (24) Zyss, J.; Oudar, J. L. *Phys. Rev. A* **1982**, *26*, 2028.
- (25) Wortmann, R.; Bishop, D. M. *J. Chem. Phys.* **1998**, *108*, 1001.
- (26) Spek, A. L. *HELENA. CAD-4 Data Reduction Program*; University of Utrecht: Utrecht, The Netherlands, 1997.
- (27) *SMART and SAINT*; Bruker AXS Inc.: Madison, WI, 2003.
- (28) Sheldrick, G. M. *Acta Crystallogr., Sect. A* **2008**, *64*, 112.
- (29) Kurtz, S. K.; Perry, T. T. *J. Appl. Phys.* **1968**, *39*, 3798.
- (30) Garcia, M. H.; Rodrigues, J. C.; Dias, A. R.; Piedade, M. F. M.; Duarte, M. T.; Robalo, M. P.; Lopes, N. J. *Organomet. Chem.* **2001**, *632*, 133.
- (31) Stewart, J. J. P. *J. Comput. Chem.* **1989**, *10*, 209.
- (32) Stewart, J. J. P. *J. Comput. Chem.* **1989**, *10*, 221.
- (33) Stewart, J. J. P. *J. Comput. Chem.* **1991**, *12*, 320.
- (34) Stewart, J. J. P. *J. Mol. Model.* **2004**, *10*, 155.
- (35) Stewart, J. J. P. *J. Mol. Model.* **2007**, *13*, 1173.
- (36) Stewart, J. J. P. *MOPAC2009*, Version 9.045W ed.; Stewart Computational Chemistry: Colorado Springs, CO, 2009.
- (37) Hamada, T. *J. Phys. Chem.* **1996**, *100*, 8777.
- (38) Böttcher, C. J. *Theory of Electric Polarization*; Elsevier: Amsterdam, The Netherlands, 1973; Vol. 1.
- (39) van Duijnen, P. T.; de Vries, A. H.; Swart, M.; Grozema, F. *J. Chem. Phys.* **2002**, *117*, 8442.
- (40) Onsager, L. *J. Am. Chem. Soc.* **1936**, *58*, 1486.
- (41) Zyss, J.; Tsoucaris, G. T. In *Structure and Properties of Molecular Crystals*; Pierrot, M., Ed.; Elsevier: Amsterdam, The Netherlands, 1990.

- (42) Humphrey, W.; Dalke, A.; Schulten, K. *J. Mol. Graphics* **1996**, *14*, 1, 33.
- (43) Macrae, C. F.; Edgington, P. R.; McCabe, P.; Pidcock, E.; Shields, G. P.; Taylor, R.; Towler, M.; van de Streek, J. *J. Appl. Crystallogr.* **2006**, *39*, 453.
- (44) Pereira Silva, P. S.; Cardoso, C.; Ramos Silva, M.; Paixão, J. A.; Matos Beja, A.; Nogueira, F. *J. Mol. Struct.* **2008**, *888*, 92.
- (45) Allen, F. H.; Kennard, O.; Watson, D. G.; Brammer, L.; Orpen, A. G.; Taylor, R. *J. Chem. Soc., Perkin Trans. 2* **1987**, S1–19.
- (46) Etter, M. C. *Acc. Chem. Res.* **1990**, *23*, 120.
- (47) Desiraju, G. R. *Nature* **2001**, *412*, 397.
- (48) Le Floch, V.; Brasselet, S.; Roch, J.-F.; Zyss, J. *J. Phys. Chem. B.* **2003**, *107*, 12403.
- (49) Brasselet, S.; Le Floch, V.; Treussart, F.; Roch, J.-F.; Zyss, J.; Botzung-Appert, E.; Ibanez, A. *Phys. Rev. Lett.* **2004**, *92*, 207401.
- (50) Brasselet, S.; Zyss, J. C. R. *Physique* **2007**, *8*, 165.
- (51) Nicoud, J. F.; Twieg, R. J. In *Nonlinear Optical Properties of Organic Molecules and Crystals*; Chemla, D. S., Zyss, J., Eds.; Academic Press: Orlando, FL, 1987; Vol. 2, p 251.
- (52) Halbout, J. M.; Blit, S.; Tang, C. L. *IEEE J. Quantum Electron.* **1981**, *QE-17*, 513.
- (53) Kleinman, D. A. *Phys. Rev.* **1962**, *126*, 1977.
- (54) Boyd, R. W. *Nonlinear Optics*, 3rd ed.; Academic Press: Burlington, MA, 2008.
- (55) *Nonlinear Optical Properties of Organic Molecules and Crystals*; Chemla, D. S., Zyss, J., Eds.; Academic Press: Orlando, FL, 1987; Vol. 2.
- (56) Kotler, Z.; Hierle, R.; Zyss, J. *J. Opt. Soc. Am. B* **1992**, *9*, 534.
- (57) Horicuhi, N.; Lefaucheux, F.; Ibanez, A.; Josse, D.; Zyss, J. *Opt. Mater.* **1999**, *12*, 351.
- (58) Horicuhi, N.; Lefaucheux, F.; Ibanez, A.; Josse, D.; Zyss, J. *J. Opt. Soc. Am. B* **2002**, *19*, 1830.
- (59) Masse, R.; Zyss, J. *Mol. Eng.* **1991**, *1*, 141.
- (60) Pécaut, J.; Lévy, J. P.; Masse, R. *J. Mater. Chem.* **1993**, *3*, 999.
- (61) Jerphagnon, J. *Phys. Rev. B* **1970**, *2*, 1091.
- (62) Jerphagnon, J.; Chemla, D.; Bonneville, R. *Adv. Phys.* **1978**, *27*, 609.
- (63) The dipole moment of an ion is not independent of origin; therefore, any reported values from a calculation must specify the origin in order to be meaningful. In this study, the dipole moments are referred to the center of mass of the ions.
- (64) Krygowski, T. M. *J. Chem. Inf. Comput. Sci.* **1993**, *33*, 70.
- (65) Krygowski, T. M.; Cyrański, M. K. *Chem. Rev.* **2001**, *101*, 1385.
- (66) Gund, P. J. *J. Chem. Educ.* **1972**, *49*, 100.

JP909005Q